이학석사 학위논문

Midwinter suppression of the Pacific storminess: A New insight from local wave activity analysis

한겨울 북태평양 폭풍성 억제현상: 지역 유한 진폭 파동 활동성을 적용한 분석

2018년 2월

서울대학교 대학원

지구환경과학부

조 형 오

Abstract

The North Pacific storm track, which is often quantified by band-passed filtered eddy variance, shows a relatively weak magnitude in midwinter than in adjacent seasons. This midwinter suppression of the North Pacific storm track is better characterized by local wave activity (LWA) and its budget. The LWA variance, applied to 250-hPa geopotential height field, well captures local waviness and its midwinter suppression. Although both cyclonic and anticyclonic wave activities contribute to the midwinter suppression, cyclonic wave activity (deepening of tough, cyclonic wave breaking and filamentation) exhibits a much more pronounced subseasonal cycle and explains about 73.6% of the midwinter suppression. The budget analysis of column-averaged LWA, computed for quasi-geostrophic potential vorticity, further revealed that North Pacific LWA is primarily controlled by the convergence of zonal LWA flux with a non-negligible contribution of non-conservative LWA source or sink.

Keywords: midwinter suppression, local wave activity, storm track

Student Number: 2016-20430

Table of Contents

1. Introduction

Daily regional weather systems in the midlatitudes are mostly dominated by fluctuations of baroclinic waves, which are related to migratory cyclones and anticyclones. Such baroclinic wave activity is notably strong in particular regions. They are generally called “storm tracks” and synoptic variability of transient eddies over the area is referred to as “storminess.” In fact, these terminologies are not perfectly appropriate to be used to describe baroclinic wave activity because “storm” refers to only cyclonic waves. In spite of this reason, we use these common terms in this study to keep consensus with the literature.

Storm tracks have important roles in synoptic meteorology and regional climate. They are closely related to severe weather in the midlatitudes, which are usually accompanying heavy rain and strong gusts that bring about substantial socioeconomic damage to affected regions. In the Northern Hemisphere, the North Pacific and the North Atlantic are two major regions of storm tracks. In previous studies, these storm tracks have been identified through synoptic-scale Eulerian statistics, which are defined as variance of bandpass filtered variables (e.g, 200 hPa geopotential height, 200 hPa meridional wind, 850 hPa meridional heatflux).

The storminess over storm tracks has peculiar characteristics that are unique to the North Pacific. According to linear dynamics, baroclinic

instability (baroclinicity) promotes baroclinic wave activities (Charney, 1947; Eady 1949; Lindzen and Farrell, 1980). Such baroclinic instability is proportional to the meridional temperature gradient (corresponds to vertical wind shear). This baroclinicity of both regions of Northern Hemispheric storm tracks (North Pacific, North Atlantic) peaks in the boreal winter because the meridional temperature gradient is maximized during winter. Consequently, from the theoretical interpretation, it is simply deducted that storminess may be maximized in winter. This is true for North Atlantic, however, North Pacific storminess is suppressed in winter rather than in autumn and spring. Such a phenomenon is called as the midwinter suppression of Pacific storminess (hereafter the midwinter suppression). A through explanation of midwinter suppression has been a puzzling issue for decades. Solving this mysterious problem is important because it can help our understanding about storm tracks which is related to synoptic weather systems of the midlatitudes. Furthermore, understanding the theory behind storm tracks can be helpful in predicting changes in regional weather, and to see whether the midwinter suppression is more dominant in the future or not.

Past research attemped to reveal the possible mechanisms of midwinter suppression. Nakamura (1992), who initially identified the midwinter suppression, suggested that extremely strong jets that

exceeded 45 m s^{-1} are negatively correlated with baroclinic wave activities. Christoph et al. (1997) also showed that midwinter suppression is also found in GCM results as well as in reanalysis data sets. Nakamura and Sampe (2002) documented that the excessively intensified subtropical jet may trap baroclinic waves in higher altitudes and reduce baroclinic growth in midwinter. Park et al. (2010) and Lee et al., (2013) demonstrated that the central Asian mountains have an important role in the midwinter suppression. Penny (2010) noted that the objectively tracked cyclones (Lagrangian perspective) exhibited suppressed activity during winter only over the Northern Pacific.

While much research has been done to find possible mechanisms about the midwinter suppression, sufficient explanations are still yet to be obtained. As mentioned above, most of these theories in the literature used Eulerian statistics to quantify baroclinic wave activity. Thus, it is not clear which wave component is more attributable to storm tracks among cyclonic and anticyclonic waves.

In this regard, a new weather diagnostic variable which can separate cyclonic and anticyclonic waves is needed. Huang and Nakamura (2016) (hereafter HN16) mathematically formulated local wave activity (LWA) in order to characterize localized weather events and diagnose eddy-mean flow interactions on regional scales. Furthermore, Chen et al. (2015) (hereafter C15) introduced LWA as a diagnostic of 500 hPa geopotential

height to identify midlatitude weather systems. It is confirmed that this LWA can be usefully employed in research of synoptic meteorology, because LWA effectively distinguishes between cyclonic and anticyclonic wave activity.

To better understand the midwinter suppression, this study verifies spatial and temporal properties of storminess over the storm tracks. In addition, budget analyses are employed to examine the dynamics over the storm tracks. As in state-of-the-art researches, LWA is used as a weather diagnostic variable. Storminess is separately calculated for cyclonic, anticyclonic and total LWA (cyclonic+anticyclonic LWA) to evaluate the contribution of each component on the midwinter suppression. Column budgets of LWA are examined to quantify the temporal variability of LWA.

2. Data and Methods

2.1 Data

This study employs 6-hourly data from the European Centre for Medium-Range Weather Forecasts Re-Analysis Interim (ERA-Interim). The ERA-Interim data have horizontal resolution of 1.5°×1.5° with 37 vertical levels from 1000 hPa to 1 hPa. Geopotential height, relative vorticity, zonal wind, meridional wind, and temperature variables from 1979 to 2016 are used in this study. Elevation data that are used in this study are ETOPO5 data, obtained from NOAA National Centers for Environmental Information with the same horizontal resolution as the ERA-Interim data.

2.2 Local wave activity

In linear wave dynamics, multiplications of deviations from zonal mean terms are neglected because amplitude of waves are assumed to be small. However, in a real atmosphere, especially for extreme weather, such terms have non-negligible impacts. Because of such limitation of linear theory, considering finite amplitude (not small amplitude) is important in studying synoptic scale waves.

Finite-amplitude wave activity (FAWA), which is developed by Nakamura and Zhu (2010) measures the waviness of quasi-geostrophic potential vorticity (QGPV) and related eddy-mean flow interactions.

However, FAWA is not suitable for analysis in local weather systems like cyclones and anticyclones because it is a zonal mean quantity. Recently, HN16 proposed LWA, which is generalized from FAWA and can express localized weather anomalies in a certain longitude. LWA quantifies meridional displacement of contours of a dynamic variable to identify anomalous troughs and ridges, which correspond to cyclonic and anticyclonic activity respectively.

As a first step in calculating LWA, the dynamic quantity q that monotonically increases or decreases along the latitude should be considered. For example, geopotential height and QGPV were used as a dynamic quantity in C15 and HN16 respectively. Here, we use both geopotential height and QGPV to calculate LWA. LWA that is calculated using geopotential height and QGPV are referred to LWA_Z and LWA_QGPV respectively.

2.2.1 LWA_Z

For the sake of simplicity, we assume that geopotential height approximately decreases with latitude, with locally reversed contours. The polar section area of geopotential height contour of value $Q(y,z)$ can be defined as $S(Q) = \iint_{q<Q} a^2 cos\varphi d\lambda d\varphi$. Here λ denotes longitude, φ is latitude, and a is the radius of Earth. Then we can define an equivalent latitude where its encircled area from the pole is the same as

$S(Q)$. This equivalent latitude is defined as $\varphi_e(Q) = \arcsin[1 - \frac{S(Q)}{2\pi a^2}]$. The eddy component of geopotential height is defined as difference between the raw field and the reference state:

$$q_e(\lambda, \varphi, \varphi', z, t) \equiv q(\lambda, \varphi + \varphi', z, t) - q_{ref}(\varphi, z, t)$$

With this definition of the eddy state, the southern and northern LWA_Z can be defined as

$$A_S(\lambda, \varphi, z, t) = \frac{a}{cos\varphi} \int_{q_e \le 0, \varphi \le \varphi_e} q_e(\lambda, \varphi, z, t) \cos\varphi \, d\varphi$$

and

$$A_N(\lambda, \varphi, z, t) = \frac{a}{cos\varphi} \int_{q_e \ge 0, \varphi \ge \varphi_e} q_e(\lambda, \varphi, z, t) \cos\varphi \, d\varphi$$

Here A_S and A_N denote LWA_Z of southward (cyclonic) and northward (anticyclonic) displacements of the Q contour from equivalent latitudes respectively. In the North Hemisphere, A_S is negative and A_N is positive by their definitions. This property is comparable to classical signs of anomalous low and high systems, which are defined by SLP or geopotential height. Thus, as in the following equation, total LWA_Z is defined as summation of two LWA_Z terms in order to diagnose synoptic weather systems and its variability.

$$A = A_S + A_N$$

C15 also documented that the summation of two LWA_Z components effectively illustrates midlatitude meteorological systems. Therefore, we

adopt total LWA_Z, cyclonic LWA_Z and anticyclonic LWA_Z to analyze each wave components' impacts on the midwinter suppression.

2.2.2 LWA_QGPV

Next, LWA_QGPV is used for more quantitative and dynamical analysis. QGPV used in this study is defined as

$$q \equiv f + \zeta + fe^{\frac{z}{H}} \frac{\partial}{\partial z}\left(e^{-\frac{z}{H}} \frac{\theta - \tilde{\theta}}{\partial \tilde{\theta}/\partial z} \right),$$

where f is planetary vorticity (Coriolis parameter), ζ is relative vorticity, z is pressure pseudo-height ($z = -H \ ln\frac{p}{p_0}$; H is scale height that assumed to 7 km, p is pressure, p_0 = 1000 hPa), θ is potential temperature, and $\tilde{\theta}$ is the hemispheric averaged potential temperature. Even the sign of the meridional gradient is opposite to the previous case, we also assume that QGPV increases with latitude to quantify LWA_QGPV. The difference between LWA_Z and LWA_QGPV is that the tendency equation (budget relation) of LWA_QGPV can be formulated unlike that of LWA_Z. This difference is because QGPV is conserved in some assumptions but geopotential height is not.

The common letters in the previous section are used here with the same context. In addition, $\varphi_e(Q)$ and $q_e(\lambda, \varphi, \varphi', z, t)$ are also defined in a same way, however, $S(Q) = \iint_{q>Q} a^2 cos\varphi d\lambda d\varphi$ is different because the meridional gradient of QGPV is opposite to that of geopotential height.

The integration of q_e in meridional direction for displacement of contours is defined to LWA _QGPV at a given longitude.

$$\tilde{A}^*(\lambda, \varphi, z, t) = -\frac{a}{cos\varphi}\int_0^{\Delta\varphi} q_e(\lambda, \varphi, z, t)\cos(\varphi + \varphi')\, d\varphi'$$

Here $\tilde{A}^*$ means LWA_QGPV, and φ' is the latitude of deviation from the reference state. In this definition, we do not distinguish between cyclonic and anticyclonic wave components in order to establish a budget analysis equation. Both equatorward and poleward displacement of isopleth contours equally correspond to positive LWA_QGPV.

The most notable point of LWA_QGPV is that budget relationship of a local tendency which is related to synoptic variability can be dynamically formulated. In order to organize the budget equation, eddy terms of wind and potential temperature are defined as follows:

$$u_e(\lambda, \varphi, \varphi', z, t) \equiv u(\lambda, \varphi + \varphi', z, t) - u_{ref}(\varphi, z, t)$$

$$v_e(\lambda, \varphi, \varphi', z, t) \equiv v(\lambda, \varphi + \varphi', z, t)$$

$$\theta_e(\lambda, \varphi, \varphi', z, t) \equiv \theta(\lambda, \varphi + \varphi', z, t) - \theta_{ref}(\varphi, z, t)$$

The reference states are acquired by analogous surface wave activity, which was defined in Nakamura and Solomon (2010). The reference state of zonal wind can be defined by the following thermal wind relationship.

$$\frac{\partial u_{ref}}{\partial z} = -\frac{R}{Ha}\frac{e^{-\kappa z/H}}{2\Omega sin\varphi}\frac{\partial \theta_{ref}}{\partial \varphi}$$

This u_{ref} is a function of latitude and vertical levels, which is calculated by integrating the equation in the vertical direction. A no slip

surface boundary condition (i.e., $u_{ref}(y,0)=0$) is used.

The derivation of the budget equation starts from the QGPV conservation equation as following:

$$\frac{dq}{dt}=\frac{\partial q}{\partial t}+u\frac{\partial q}{\partial x}+v\frac{\partial q}{\partial y}=0$$

By integrating the above formula in the meridional direction, we get the LWA_QGPV tendency equation in a certain level. The density-weighted column averaging and boundary conditions which assume negligible meridional heat flux at the top of the atmosphere are employed to the tendency equation and result in the establishment of the column budget as follows:

$$\frac{\partial}{\partial t}\langle\tilde{A}^{*}\rangle cos\varphi = -\frac{1}{a}\frac{\partial F_A}{\partial\lambda}+\frac{1}{acos\varphi}\frac{\partial}{\partial\varphi'}(\langle u_e v_e cos^2(\varphi+\varphi')\rangle)+\frac{f cos\varphi}{H}\left(\frac{v_e\theta_e}{\partial\tilde{\theta}/\partial z}\right)_{z=0}+\langle\dot{\tilde{A}}^{*}\rangle\, cos\varphi$$

$\langle(\cdot)\rangle$ denotes the density-weighted column averaged value of the variable. Zonal LWA (F_A) is defined as follows:

$$F_A = \langle u_{ref}\tilde{A}^{*}\rangle-\frac{a}{\cos\varphi}\langle\int_0^{\Delta\varphi}u_e\, q_e\cos(\varphi+\varphi')\,d\varphi'\rangle$$

$$+\frac{1}{2}\langle v_e^2-u_e^2-\frac{R}{H}\frac{e^{-\frac{\kappa z}{H}}\theta_e^2}{\partial\tilde{\theta}/\partial z}\rangle$$

In the budget equation, the left hand side represents the local tendency of LWA with cosine latitude weighting. The first term on the right hand side is the zonal LWA flux convergence. The second term denotes meridional eddy momentum flux divergence. The third term is the low-level meridional heat flux. Finally, the last term denotes a

residual term, which is not originally derived from the equation. The residual term contains non-conservative, diabatic, non-QG and truncation errors. Detailed information of LWA_QGPV and budgets are described in HN16 and Huang and Nakamura (2017) (hereafter HN17).

2.3 Analysis techniques

Many previous studies defined baroclinic wave activity (hereafter storminess for consistency) as a variance of meteorological variables. Most of them used band/high-pass filtered variance or employed 24-hr difference filters to calculate synoptic-scale variability. In this study, we employ a 24-hour difference filter to quantify synoptic-scale variance.

$$\overline{X'^2} = \overline{[X(t+24hr) - X(t)]^2}$$

Here, X denotes a variable of analysis (e.g. geopotential height, LWA_Z). A variance applying the 24-hr difference filter can be used to define storminess, because it eliminates long-term variability, which acts as a highpass filter to analyze short-term waves (Wallace et al., 1988; Chang et al., 2002). This expression allows for the ease of calculations and for the physical meaning to remain consistent (Chang and Fu, 2002).

The fast Fourier transformation and its inverse transform are also exploited to separate large-scale waves and synoptic-scale waves. Here, a criterion of wavenumbers from 1 to 4 are used as large-scale waves and wavenumbers larger than 5 are used for synoptic-scale waves.

The domains of the North Pacific and North Atlantic are [30°-60°N, 160°-200°E] and [30°-60°N, 290°-330°E] respectively. All results are expressed by a 30-day moving average. The baroclinic instability is calculated using the Eady growth rate.

3. Results

3.1 Classical perspective of storminess

Figure 1 shows the climatology of the monthly mean geopotential height, zonal wind, and storminess of geopotential height at the 250 hPa level during November, February and April for 1980-2015. It is easily confirmed that 250 hPa jets over the North Pacific and North Atlantic are the strongest during February (Figs 1a-c). This implies that baroclinicity is the highest during winter compared to neighboring seasons, nevertheless these results are only for a month of each seasons (seasonal mean results are qualitatively same, not shown). Figures 1d-1f illustrate the storminess by employing the 24-hour difference filter. The Storminess exhibit large values downstream of jet in figs 1a-1c, which is qualitatively agreed with the patterns in previous studies. The horizontal pattern of storminess well represents the region of high activity in synoptic variability, which is known as storm tracks (Hoskins and Valdes, 1990; Christoph et al., 1997; Chang and Fu, 2002; Chang et al., 2002; Hoskins and Hodges, 2002). However, the storminess is relatively

suppressed in February over the North Pacific despite the maximum intensity of the jet.

Prior to a detailed investigation of the temporal evolution of storminess, it is necessary to verify impacts of horizontal scale on storminess. Figure 2 illustrates which wave components are highly related to storminess at November, February, and April. The storminess of large-scale waves is not large and does not exhibit significant monthly variations over the storm tracks. On the other hand, waves that are smaller than or equal to the synoptic-scale have quite large variability, and exhibit relatively small storminess in February rather than November and April. Such results show that the midwinter suppression is mainly driven by waves that are smaller or equal to the synoptic-scale, and not by large-scale waves.

To examine the successive evolution of storminess, Fig. 3 depicts seasonal and meridional variations of longitudinally averaged storminess over the North Pacific (160-200°E) and the North Atlantic (290-330°E). Over the North Pacific, storminess of total waves peaks twice in autumn and spring, while it is relatively minimized in the midwinter. Unlike the North Pacific, the North Atlantic storminess exhibits a single maximum during winter. Also, these results are remarkably different by their horizontal scale of waves. Large-scale waves does not show noteworthy variations in storminess, while smaller

waves show qualitatively very similar structures as total waves about their storminess.

Figure 4 show time series of area-averaged storminess over the North Pacific and the North Atlantic. Again, over the North Pacific, storminess clearly exhibits relative minimum in midwinter rather than spring and autumn (Fig. 4a), while storminess over the North Atlantic is maximized during winter (Fig. 4d). By separating into large-scale and small or equal to synoptic-scale waves, it can be seen that storminess mainly comes from smaller scale waves. These overall features clearly imply that a large portion of variation in total storminess is mainly caused by synoptic-scale waves. This implies that these waves dominate the contribution to the midwinter suppression as noted in the literature.

Although not shown in this paper, the square root of the envelope function that is used in N92 can be used, to verify the sensitivity definition of storminess. Then, results from the 24-hour difference filtering and results that followed the methodology of N92 show qualitatively equivalent characteristics (Figs. 2-4).

3.2 Local wave activity

3.2.1 LWA_Z

All analyses in this subsection are confined to waves that are smaller than large-scale waves (wavenumbers larger than 5) because it is

confirmed that storminess of large-scale waves is not noticeable. Figure 5 shows the spatial distribution of the climatic storminess computed from LWA_Z. Figure 5a shows the regions of strong wave activity, which are well-agreed with the storm tracks that were identified in numerous previous studies. In fact, although not shown in this paper, it is also confirmed that the baroclinic wave activity calculated by Eulerian statistics, and the storminess of the LWA_Z is analyzed. Both of them exhibit qualitatively consistent results. As shown in Figs. 5a and 5b, the storminess of the total LWA_Z are generally consistent with the storminess of the cyclonic LWA_Z. Therefore, as shown in previous studies, it can be understood that the baroclinic wave activity is described as cyclone activity. However, Figs. 5b, and 5c imply that it is hard to neglect the storminess of anticyclonic LWA_Z. Even though cyclonic LWA_Z is much larger than anticyclonic LWA_Z, anticyclonic LWA_Z still has non-negligible impact.

Figure 6 shows the storminess of LWA_Z over the North Pacific and the North Atlantic, which is comparable to Fig. 3. Over the North Pacific, the storminess of total LWA_Z is maximized in the middle of October and early May, while relative minimum is observed in February. The left panels of Figs. 6a-c show that a large portion of total storminess is due to cyclonic waves, though anticyclonic waves are partly responsible. In Figs. 6d-6f, storminess over the North Atlantic uniquely peaks in the winter,

however, fairly large storminess appears around 50°N in the middle of June, which was not found in previous analysis. This signal is interesting because it is reported that the North Atlantic storminess during the boreal summer of the North Hemisphere is not so strong. This can be discussed in a further study.

Figures 7 illustrates the storminess of LWA_Z over the North Pacific and the North Atlantic for each wave component. It can be clearly observed that the storminess of total LWA_Z remarkably decreases from the middle of October, and hits a minimum during the winter, but steeply increases from early spring. The magnitude that contributes to the midwinter suppression is much larger in cyclonic LWA_Z, while the storminess of anticyclonic LWA_Z is non-negligible. Storminess of cyclonic LWA_Z dominantly explains seasonal suppression and recovery of total storminess to about 73.6%. Over the North Atlantic, storminess of each wave component exhibit a single peak during the winter like previous results.

3.2.2 LWA_QGPV

In this section, we analyze the properties of column-averaged LWA_QGPV and its budget equation. The analysis is conducted only for winter, because the LWA_Z, as shown in the previous subsection, is able to successfully identify the midwinter suppression. Unlike previous

analysis, we employ unfiltered QGPV fields to calculate LWA_QGPV because there can be unknown source or sink terms in the budget equation if it is spatially filtered.

Before performing the analysis for unfiltered variables, we examine the variance of non-filtered geopotential height over the North Pacific and North Atlantic. Figure 8 shows that raw variability is also suppressed in the winter over the North Pacific. This suggests that it is possible to explain the midwinter suppression if we used unfiltered data.

Figure 9 shows climatology of the LWA_QGPV in the wintertime. Total LWA_QGPV containing both stationary and transient waves is shown in Fig. 9a. Overall LWA_QGPV is strong over Northeast Asia, Northeast America, and Northwest Europe. Stationary LWA_QGPV is depicted in Fig. 9b and LWA_QGPV from the transient eddy component is illustrated in Fig. 9c. It is confirmed that the transient component of LWA_QGPV is high over the North Pacific, Northeast Atlantic, and continental Europe. These results qualitatively agree with the storm tracks from previous studies.

3.3 Budget analysis

Figure 10 shows the results of each term in the column budget of LWA_QGPV for the winter season. Since the LWA_QGPV is close to zero during winter, the residual term is in balance with the sum of the

remaining three terms (zonal LWA flux convergence, meridional eddy momentum flux divergence and low-level heat flux). Over the North Pacific region, the zonal LWA flux convergence is positive, which corresponds to increasing LWA. The meridional eddy momentum flux divergence is so negative that it decreases the overall LWA over the North Pacific with a change in sign around 50° N latitude. The low-level meridional heat flux usually increases LWA_QGPV because it is almost positive over most of the Northern Hemisphere. The residual term considerably reduces LWA_QGPV over the North Pacific, which includes non-conservative, non-QG, diabatic process and truncation error may impact to the midwinter suppression.

In order to quantitatively compare temporal characteristics of column budgets of LWA for the North Pacific and the North Atlantic, the domain-averaged budgets are presented Fig. 11. The most prominent difference between the two domains is the zonal LWA flux convergence. Over the North Pacific, zonal LWA flux convergence is increased during winter while the North Atlantic is nearly zero. On the other hand, the residual term is a large negative value in winter over the North Pacific and not so much over the North Atlantic Ocean.

4. Summary and Discussion

This study examines the midwinter suppression of North Pacific storminess as a new perspective through employing the LWA. The storminess of a geopotential height well indicates storm tracks and its suppression in midwinter, which is dominated by synoptic-scale waves. Storminess of LWA_Z successfully illustrates storm tracks through each wave component. Although storminess by anticyclonic LWA is relatively minimized during the winter, cyclonic LWA is much more dominant in its contribution to the midwinter suppression. The column budgets imply that wintertime LWA_QGPV over the North Pacific is substantially controlled by zonal LWA flux convergence and the residual term.

We intend to carry out a further study on whether the difference of temporal evolution in column budgets over two storm tracks contribute to the midwinter suppression of North Pacific storminess. To verify more detailed factors of the midwinter suppression, establishing modified budget equations, examining the vertical structure, and investigating interannual variabilities would be constructive.

5. Reference

Chang, E. K., and Y. Fu, 2002: Interdecadal variations in Northern Hemisphere winter storm track intensity. Journal of Climate, 15, 642-658.

Chang, E. K., S. Lee, and K. L. Swanson, 2002: Storm track dynamics. Journal of Climate, 15, 2163-2183.

Charney, J. G., 1947: The dynamics of long waves in a baroclinic westerly current. Journal of Meteorology, 4, 136-162.

Chen, G., J. Lu, D. A. Burrows, and L. R. Leung, 2015: Local finite-amplitude wave activity as an objective diagnostic of midlatitude extreme weather. Geophysical Research Letters, 42.

Christoph, M., U. Ulbrich, and P. Speth, 1997: Midwinter suppression of Northern Hemisphere storm track activity in the real atmosphere and in GCM experiments. Journal of the atmospheric sciences, 54, 1589-1599.

Eady, E. T., 1949: Long waves and cyclone waves. Tellus, 1, 33-52.

Hoskins, B. J., and P. J. Valdes, 1990: On the existence of storm-tracks. Journal of the atmospheric sciences, 47, 1854-1864.

Hoskins, B. J., and K. I. Hodges, 2002: New perspectives on the Northern Hemisphere winter storm tracks. Journal of the Atmospheric Sciences, 59, 1041-1061.

Huang, C. S., and N. Nakamura, 2016: Local finite-amplitude wave activity as a diagnostic of anomalous weather events. Journal of the Atmospheric Sciences, 73, 211-229.

Huang, C. S., and N. Nakamura, 2017: Local wave activity budgets of the wintertime Northern Hemisphere: Implication for the Pacific and Atlantic storm

tracks. Geophysical Research Letters, 44, 5673-5682.

Lee, S.-S., J.-Y. Lee, K.-J. Ha, B. Wang, A. Kitoh, Y. Kajikawa, and M. Abe, 2013: Role of the Tibetan Plateau on the annual variation of mean atmospheric circulation and storm-track activity. Journal of Climate, 26, 5270-5286.

Lindzen, R., and B. Farrell, 1980: A simple approximate result for the maximum growth rate of baroclinic instabilities. Journal of the atmospheric sciences, 37, 1648-1654.

Nakamura, H., 1992: Midwinter suppression of baroclinic wave activity in the Pacific. Journal of the Atmospheric Sciences, 49, 1629-1642.

Nakamura, H., and T. Sampe, 2002: Trapping of synoptic-scale disturbances into the North-Pacific subtropical jet core in midwinter. Geophysical Research Letters, 29, 8-1 - 8-4

Nakamura, H., and A. Solomon, 2010: Finite-amplitude wave activity and mean flow adjustments in the atmospheric general circulation. Part Ⅰ: Quasigeostrophic theory and analysis. Journal of the atmospheric sciences, 67, 3967-3983

Nakamura, N., and D. Zhu, 2010: Finite-amplitude wave activity and diffusive flux of potential vorticity in eddy–mean flow interaction. Journal of the Atmospheric Sciences, 67, 2701-2716.

Park, H.-S., J. C. Chiang, and S.-W. Son, 2010: The role of the central Asian mountains on the midwinter suppression of North Pacific storminess. Journal of the Atmospheric Sciences, 67, 3706-3720.

Penny, S., G. H. Roe, and D. S. Battisti, 2010: The source of the midwinter suppression in storminess over the North Pacific. Journal of Climate, 23, 634-

648.

Wallace, J. M., G.-H. Lim, and M. L. Blackmon, 1988: Relationship between cyclone tracks, anticyclone tracks and baroclinic waveguides. Journal of the atmospheric sciences, 45, 439-462.

6. Figures

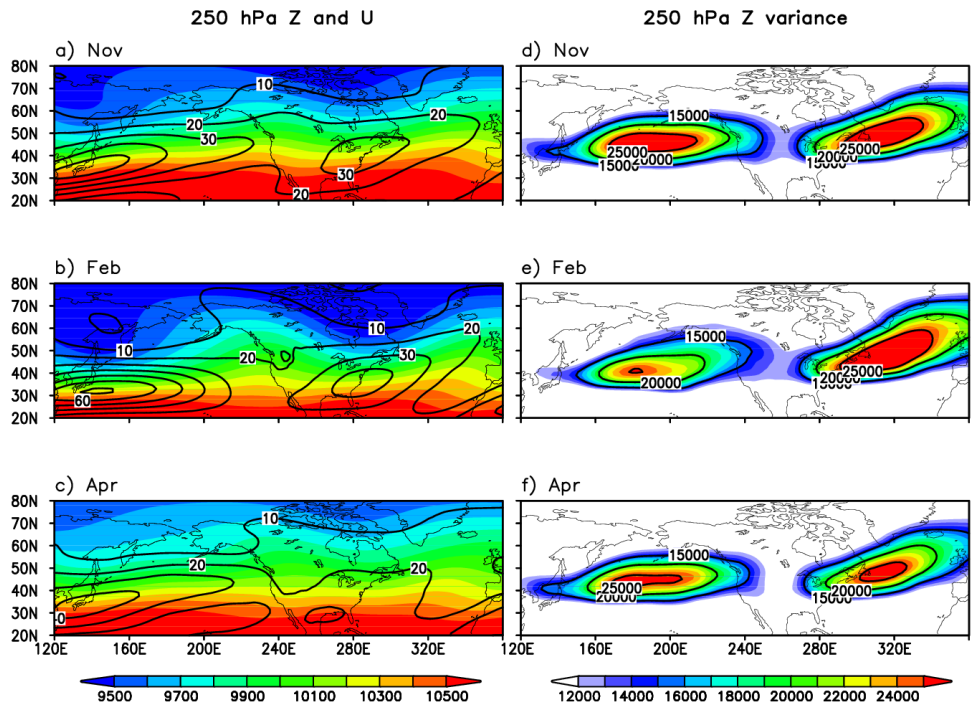

Figure 1. Horizontal distributions of geopotential height (a-c, shading, m), zonal wind (a-c, contour, $\mathbf{m}\ s^{-1}$) and 24 hour difference filtered variance of geopotential height (d-f, contour, m^2) at 250 hPa for November (a, d), February (b, e) and April (c, f). Contour intervals are $\mathbf{10}\ \mathbf{m}\ s^{-1}$in (a)-(c) and $\mathbf{2500}\ m^2$ in (d)-(f).

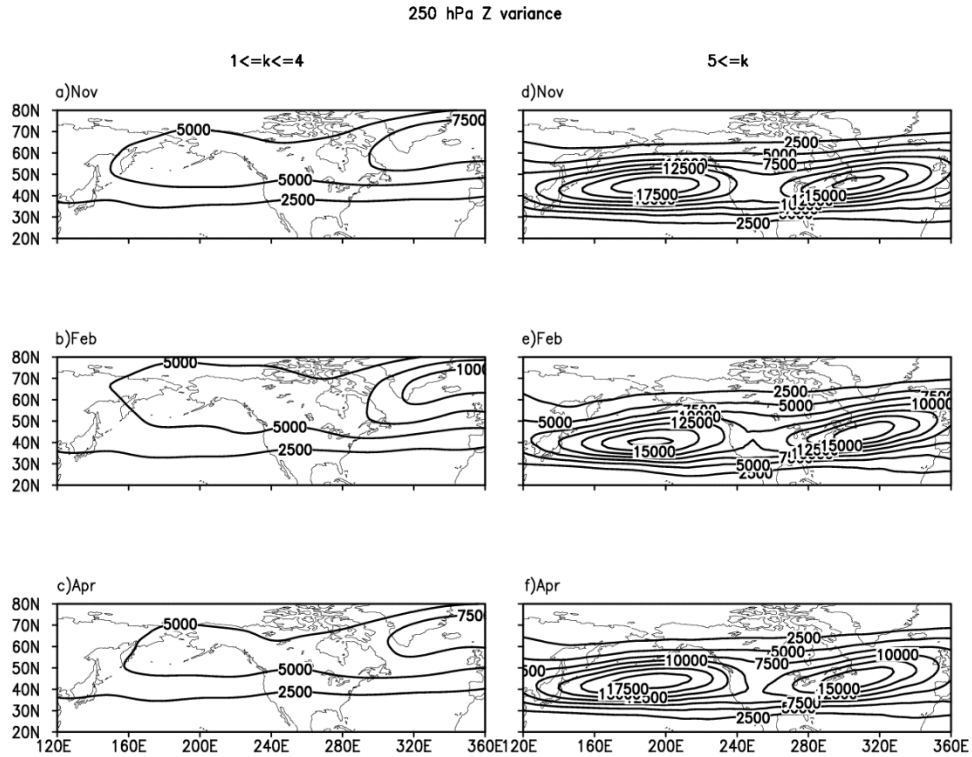

Figure 2. Horizontal distributions of 24 hour difference filtered variance of geopotential height for large-scale waves (a-c, m^2) and for synoptic-scale waves (d-f, m^2) at 250 hPa for November (a, d), February (b, e) and April (c, f).

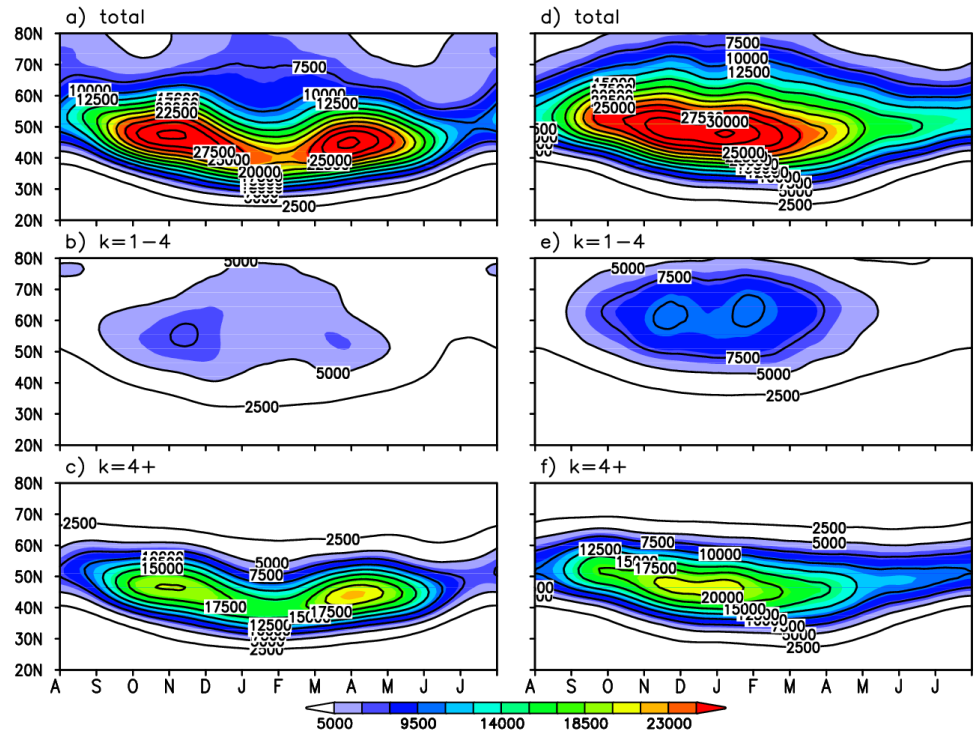

Figure 3. Seasonal march of 24 hour difference filtered variance of geopotential height for total waves (a, d, m^2), large-scale waves (b, e, m^2) and synoptic-scale waves (c, f, m^2) at 250 hPa for central pacific (a-c) and atlantic (d-f) domain.

.

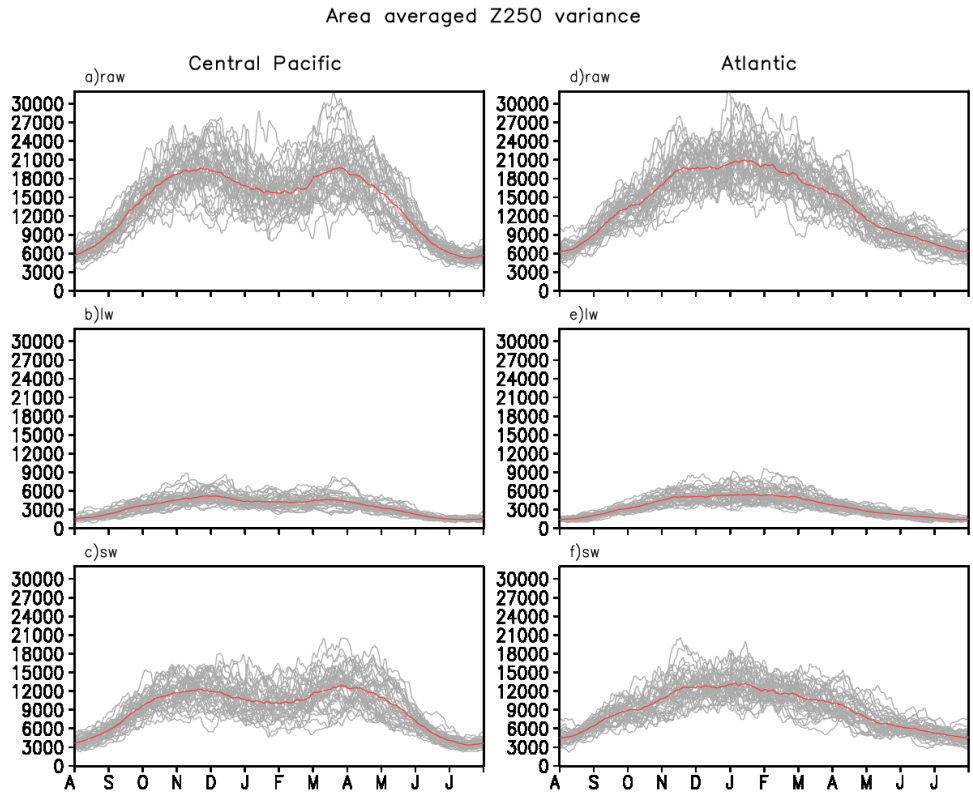

Figure 4. Monthly variation of area-averaged 24-hour difference filtered variance of geopotential height for total waves (a, d, m^2), large-scale waves (b, e, m^2) and synoptic-scale waves (c, f, m^2) at 250 hPa for central pacific (a-c) and atlantic (d-f) domain.

.

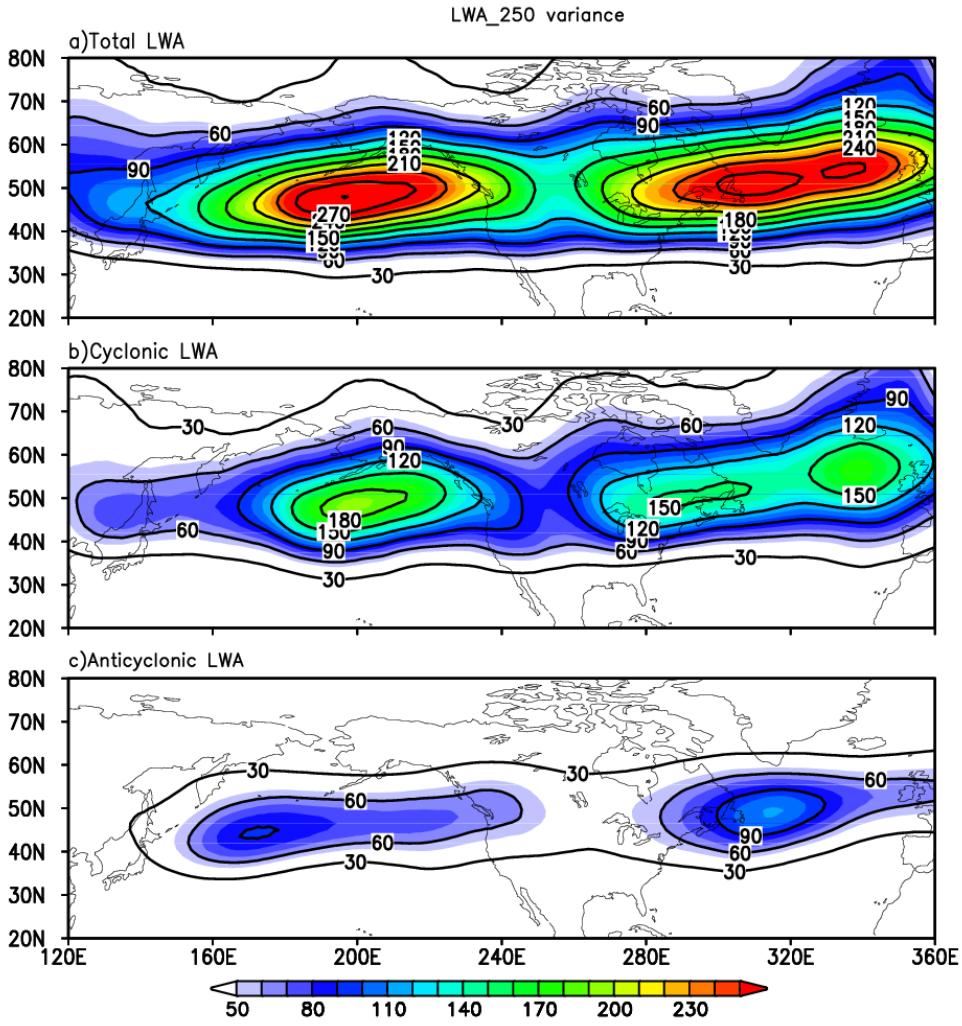

Figure 5. Horizontal distributions of 24-hour difference filtered variance of total LWA (a, $\mathbf{10^{12}}\boldsymbol{m^4}$), cyclonic LWA (b, $\mathbf{10^{12}}\boldsymbol{m^4}$) and anticyclonic LWA (c, $\mathbf{10^{12}}\boldsymbol{m^4}$) at 250 hPa.

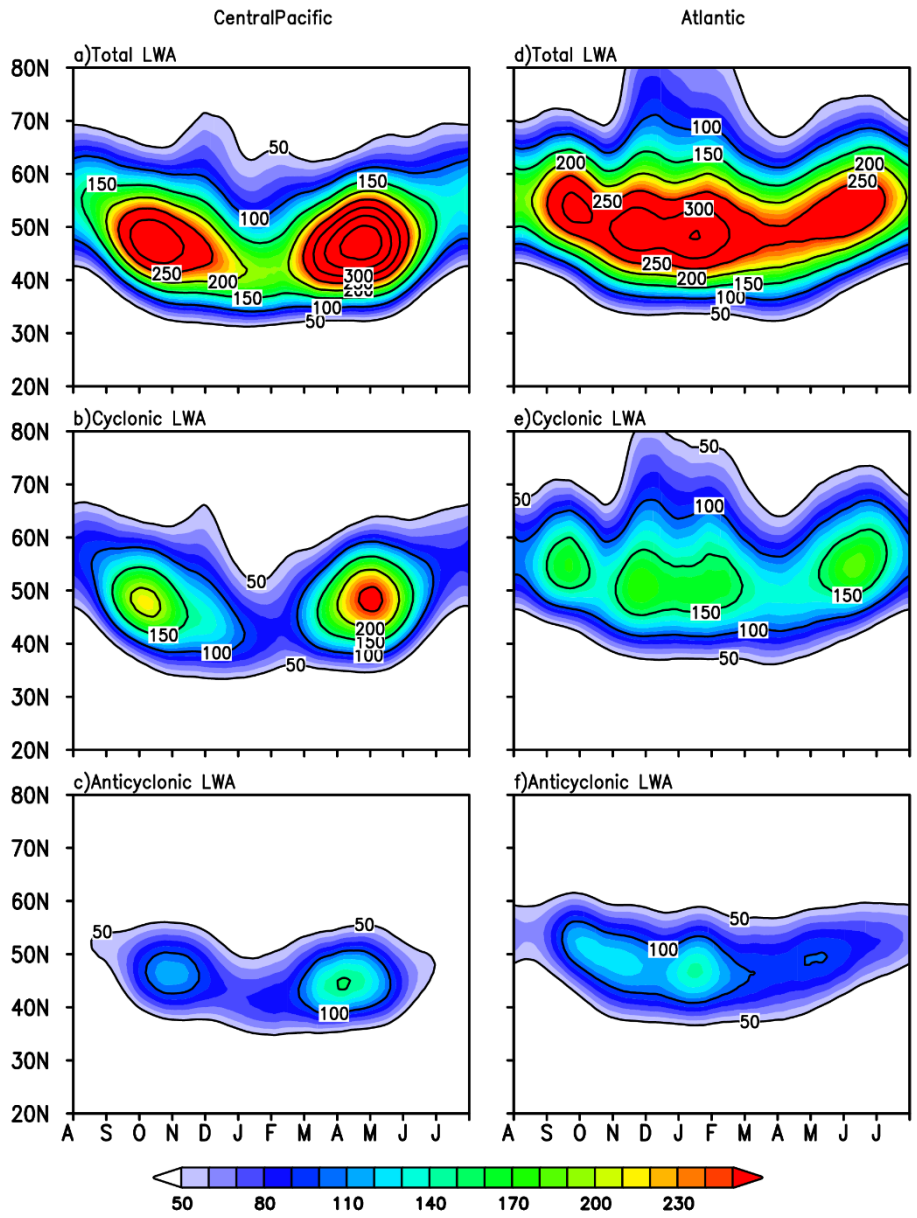

Figure 6. Seasonal march of 24-hour difference filtered variance of total LWA (a, d, $10^{12}m^4$), cyclonic LWA (b, e, $10^{12}m^4$) and anticyclonic LWA (c, f, $10^{12}m^4$) at 250 hPa for central pacific (a-c) and atlantic (d-f) domain. LWA is computed using spatially filtered geopotential height.

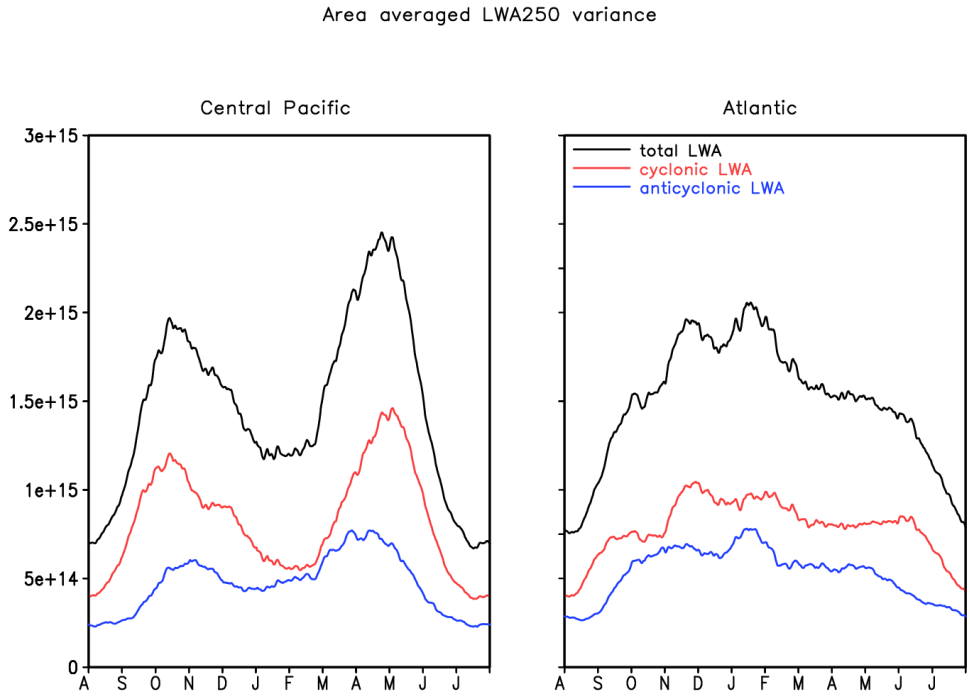

Figure 7. Monthly variation of area averaged 24-hour difference filtered variance of LWA over Central Pacific (left, m^4) and Atlantic (right, m^4) at 250 hPa.

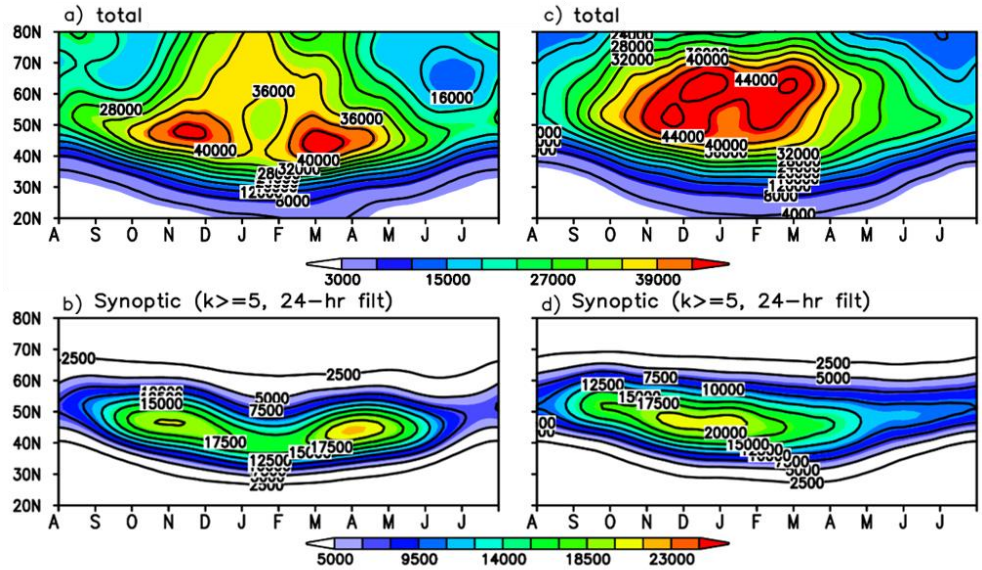

Figure 8. Seasonal march of variance in time for total waves (a, c, m^2), 24-hour difference filtered variance of synoptic-scale waves(b, d, m^2) at 250 hPa geopotential height for central pacific (a, c) and atlantic (b, d) domain.

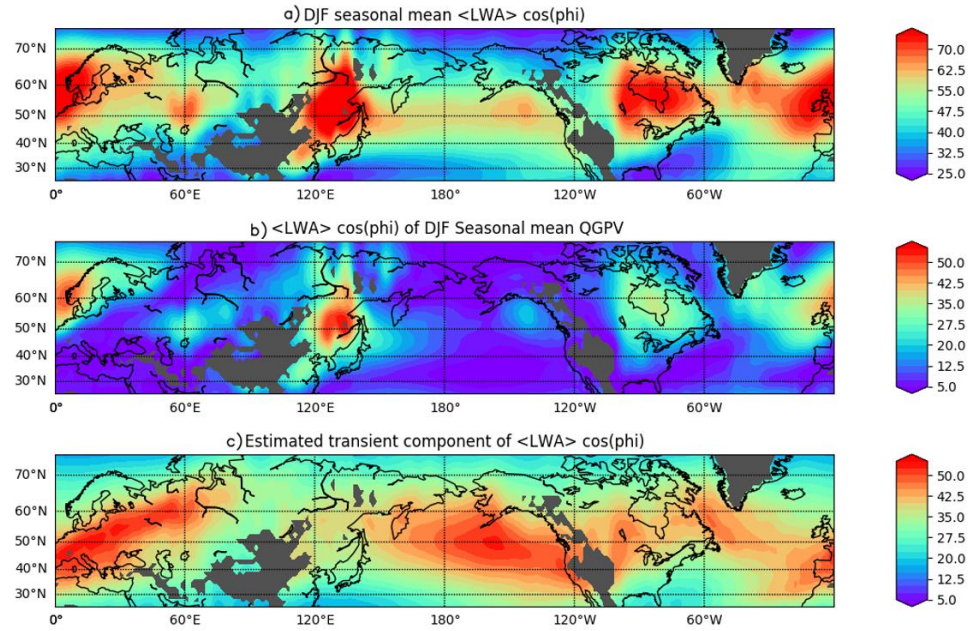

Figure 9. Horizontal distributions of seasonal mean column-averaged LWA (a, $m\ s^{-1}$), column-averaged LWA of seasonal mean QGPV (b, $m\ s^{-1}$) and estimated transient component of column-averaged LWA (c, $m\ s^{-1}$) in boreal winter.

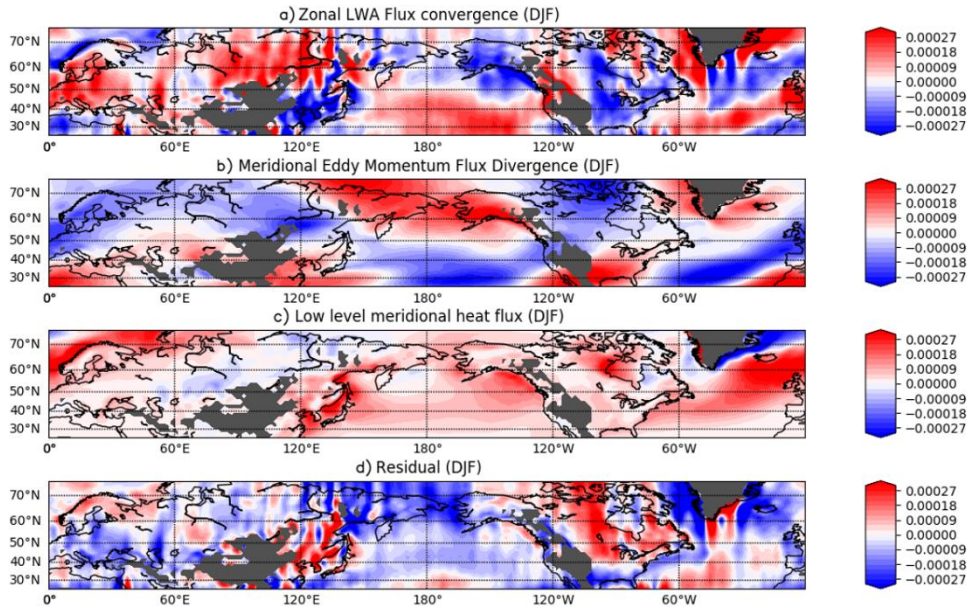

Figure 10. Horizontal distributions of seasonal mean zonal LWA flux convergence (a, $\boldsymbol{m\ s^{-1}day^{-1}}$), meridional eddy momentum flux divergence (b, $\boldsymbol{m\ s^{-1}day^{-1}}$), low-level meridional heat flux (c, $\boldsymbol{m\ s^{-1}day^{-1}}$) and residual (d, $\boldsymbol{m\ s^{-1}day^{-1}}$) in boreal winter.

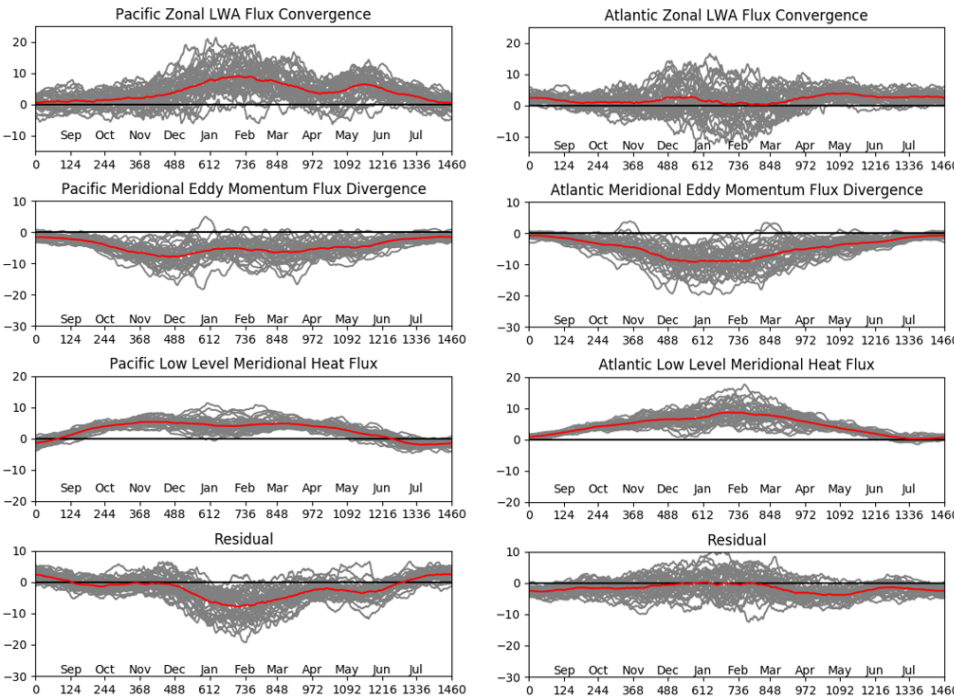

Figure 11. Monthly variation of area averaged budgets over the central Pacific (left, $\boldsymbol{m\ s^{-1}day^{-1}}$) and Atlantic (right, $\boldsymbol{m\ s^{-1}day^{-1}}$).

초 록

한겨울 북태평양 폭풍성 억제현상: 지역 유한 진폭 파동 활동성을 적용한 분석

조형오
지구환경과학부
석사과정
서울대학교

북태평양 폭풍 경로는 주로 변수들의 에디 변동성으로 정의되며, 한겨울철에 그 크기가 가을과 봄철에 비해 상대적으로 약하다. 이런 북태평양 폭풍성 억제현상은 지역 파동 활동성과 수지 분석을 통해 특징이 보다 잘 이해된다. 250 hPa 지위고도장에서 계산된 지역 파동 활동성의 변동성은 지역적 파동성과 한겨울의 폭풍성 억제현상을 잘 진단한다. 저기압성, 고기압성 파동 활동성이 모두 한겨울 폭풍성 억제현상에 기여하지만 저기압성 파동 활동성이 훨씬 더 두드러진 계절간 변동을 보여 폭풍성 억제의 약 73.6%를 설명한다. 준지균 잠재와도를 적용해 계산한 지역 파동 활동성을 연직방향으로

적분하여 이 파동 활동성의 시간적 변화에 대한 수지 관계식을 구성할 수 있다. 이 수지 분석의 결과, 주로 동서방향 지역 파동 활동성 플럭스의 수렴과 무시할 수 없는 비보존항들에 의해 북태평양 지역 파동 활동성이 주로 지배되었다.

주요어: 한겨울 폭풍성 억제, 지역파동 활동성, 폭풍경로

학번: 2016-20430